Back Focal Plane Computation Method for grating surface under Optical Microscope for sensing application

Suvicha Sasivimolkul, Chayanisa Sukkasem, Phitsini Suvarnaphaet and Suejit Pechprasarn*

College of Biomedical Engineering, Rangsit University, Pathum Thani, Thailand
*Corresponding author, E-mail: suejit.p@rsu.ac.th

Abstract

This paper shows an implementation of a back focal plane image with and without a grating structure on the surface of a sensor-based surface plasmon resonance. The simulation method is based on a back focal plane of a focal point scanning reflection microscope. Then, a focal point position was taken into account under the proposed calculation. The authors measured qualitative parameters from the surface plasmon-based Kretschmann configuration with and without a dielectric grating in an application. The results showed that the surface plasmon sensor with a modified grating on the surface has higher merit than 20 times. The perspective of this paper has promised the sensor-based surface plasmon resonance and establishes an architecture for enhancing bioanalysis of plasmonic applications.

Keywords**:** *Back Focal Plane, Optical sensor, Surface Plasmon Resonance, Grating*

1. Introduction

The existence of a back focal plane (BFP) image of a microscope objective gives various applications, for instance, sub-nanometer resolution for single-molecule imaging (Nugent-Glandorf & Perkins, 2004), enhancement of optical tweezers (Gittes & Schmidt, 1998), phase contrast microscopy (Mann et al., 2005), and optical mode analysis (Pechprasarn et al., 2014). Moreover, the BFP image can provide material properties (Shen et al., 2020) such as refractive index and thickness, if a surface plasmon (SP) sensor (Suvarnaphaet & Pechprasarn, 2018) was chosen. (Couture et al., 2013) Regarding the use of BFP in biological sensing, to the author's knowledge, the calculation method of the back focal plane image with the grating surface has not been reported before.

The SP sensor is the optical biosensor-based surface plasmon resonance (SPR) (Schasfoort, 2017). The SPR exploits particular electromagnetic waves or surface plasmon polaritons (SPPs) confined to its surface to probe the change in the analyte's refractive index in solution and a biomolecular recognition immobilized on the SPR sensor surface (Johnsson et al., 1991). Therefore, the surface plasmon resonance measurement has been widely used in bacteria detection in foodstuffs (Pechprasarn et al., 2019), proteins and drugs (Thillaivinayagalingam et al., 2010), and environmental pollutions (Mahmoudpour et al., 2019). Besides, in the last few decades, SPR phenomena have been invented as a surface plasmon microscopy (SPM) (Rothenhäusler & Knoll, 1988) and combined with another imaging technique to be widefield-SPM (Stabler et al., 2004) and confocal-SPM (Pechprasarn & Somekh, 2014).

There are several configurations of the SPR sensors that are capable of generating and measuring surface plasmon resonance. Firstly, the prism-based coupling, the two well-known configurations, which include Kretschmann configuration (Kretschmann & Raether, 1968) and Otto configuration (Otto, 1968). These two configurations are based on the attenuated total reflection (ATR) method to excite the SPR, the schemes shown in Figure 1(a) and 1(b), respectively. There is a bit of difference between them due to the space (d_{otto}) between the metal and prism. Secondly, the grating-based coupling, the grating architecture shown in Figure 1(c), has been provided diffraction of the incident light to excite the SPR (Ritchie et al., 1968). The grating-based coupling gives a high sensitivity (Dai et al., 2018) and high resolution (Hu, 2011) compared with the prism-based coupling (Homola et al., 1999).

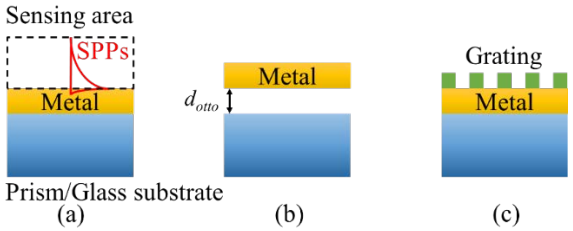

Figure 1 (a) Kretschmann configuration, (b) Otto configuration, and (c) Grating-assisted SP sensor

A BFP analysis has become a powerful tool in science, especially combined with the SPR measurement. In this paper, the flow of the story will be arranged according to the following:

1) An implementation of BFP imaging under a focal point scanning reflection microscope would be presented.
2) A grating-assisted SP sensor based on Kretschmann configuration would be chosen for a refractive index sensing application.

2. Objectives

1) To implement the BFP image from a dielectric grating-assisted SP sensor based on Kretschmann configuration under a focal point scanning reflection microscope.

2) To determine the concentration of the analyte solution by refractive index sensing.

3. Materials and Methods

3.1 The focal point scanning reflection microscope

To study the BFP image, the authors introduced the focal point scanning reflection microscope's schematic shown in Figure 2. The sample was illuminated by linear polarized light with the incident wavelength λ_0 of 633nm (Nelson et al., 1999), and the reflected light from the sample was collected by the objective lens. A polarizer or $\lambda/2$ waveplate was used to select s-polarization (E_y component) and p-polarization (E_x component) or to adjust the p-polarization to be a horizontal line position. A CCD camera was used to capture the BFP image. Note that, XY sample stage scanner is not shown in the drawing.

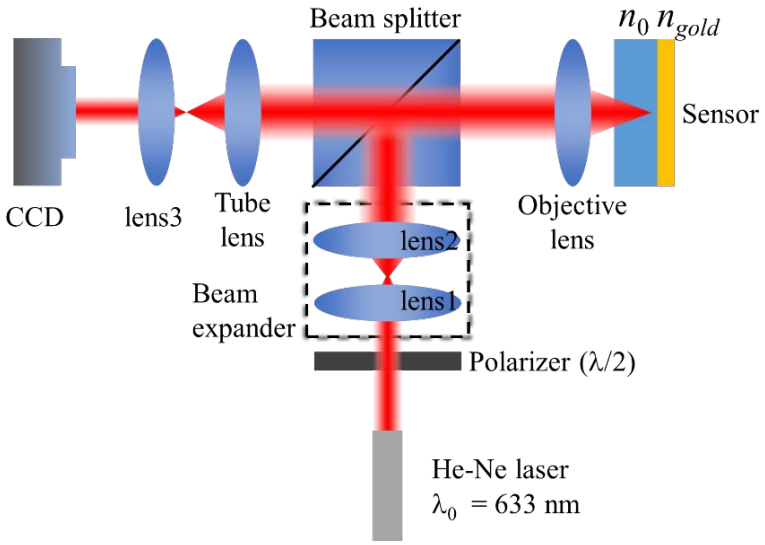

Figure 2 A schematic of the system used to capture the back focal plane

This system allows the reflectivity over an extensive range of incident angles, which depend on a numerical aperture (NA) of an objective lens. The BFP of a microscope objective illuminating on a 48-nm gold film/Glass substrate (n_0=1.52) based Kretschmann configuration in the air using a 1.49 NA objective lens at 633 nm wavelength was shown in Figure 3(a), and its character is shown in Figure 3(b).

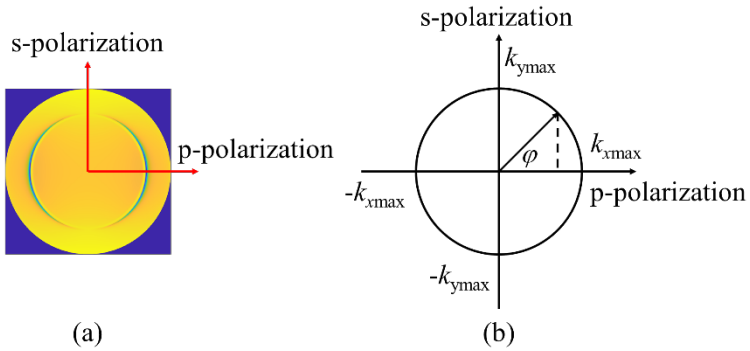

Figure 3 (a) the calculated BFP image reflected from a gold sample in the air using 1.49 NA objective lens and (b) the characteristics of the BFP

Figure 3(a) shows the amplitude of the calculated BFP with the SPR respond dip in the x-direction (p-polarization). The detailed BFP calculation for the uniform film has been discussed by Pechprasarn *et al.* (Pechprasarn & Somekh, 2012). If the sensor was illuminated by an incident light or incident wave vector (k_{inc}), the maximum wave vector in x (k_x) and y (k_y) direction were [$-k_{xmax}$, k_{xmax}] and [$-k_{ymax}$, k_{ymax}], respectively, where $k_{x\max} = k_{y\max} = \text{NA}$ of an objective lens and polarization angle φ is relative of arctan k_y/k_x and the calculation of k_x and k_y at any incident angle shows below:

$$k_x = k_y = \frac{2\pi}{\lambda_0} n_0 \sin(\theta) \tag{1.1}$$

3.2 Calculation of Back Focal Plane

The reflected light or reflection coefficient (r) from the uniform sample, even the multi-layer uniform sample could be calculated using the Fresnel equations and Transfer matrix method (Pechprasarn & Albutt, 2019). The reflected light of the microscope objective illuminating a sample contains the reflection coefficient of p-polarization (r_p) and s-polarization (r_s). Electric field components could calculate the manipulation of the BFP image as follows:

(1) Calculate the reflection coefficient r_s and r_p from Fresnel equations.

(2) Calculate the electric field components.

$$E_x = r_p \cos(\varphi) - r_s \sin(\varphi) \tag{1.2}$$

$$E_y = r_p \sin(\varphi) + r_s \cos(\varphi) \tag{1.3}$$

(3) Calculate the BFP image with a uniform sample by a summation of the intensity of E_x and E_y components.

$$BFP = E_{total} = \left|E_x\right|^2 + \left|E_y\right|^2 \tag{1.4}$$

However, suppose a grating structure was chosen to enhance the figure of merit (FoM) or the sensor's quality, in that case, the reflection coefficient r_s and r_p could, therefore, be calculated by rigorous coupled-wave analysis (RCWA) (Moharam et al., 1995). Then, assuming it was one-directional grating and its grating direction or the grating wave vector (k_g) was in k_x direction, the BFP image would be taken all grating wave vectors into account. The visualization of the grating wave vector was shown in Figure 4(a).

The black-circle (0th order) is a BFP at zero-order diffraction. If there has a diffraction grating, the 0th order will interfere with other diffractions. For example, the 0th order will interfere with the red-dotted circle (1st order and -1st order) enormously due to the nearest order, and the 0th order then interferes gradually decrease in amplitude with 2nd and -2nd, then 3rd and -3rd, …, mth and -mth. Figure 4(b) shows the grating-assisted SP sensor-based Kretschmann configuration with the different focal point (x_{pos}) of the objective lens; (i) the focus is on the center of grating material (n_1) and (ii) the focus is on the center of a sample (n_2).

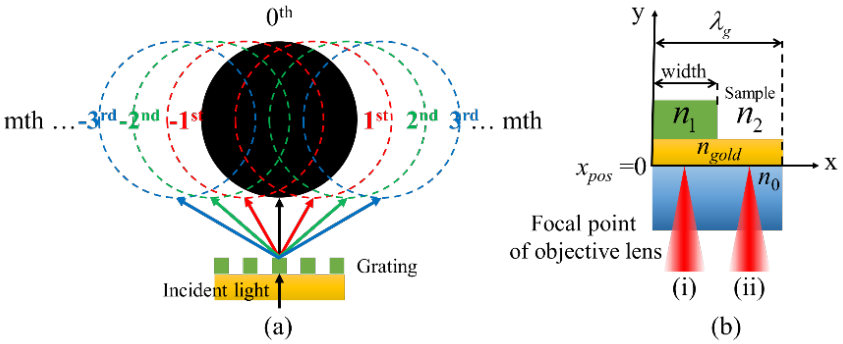

Figure 4 (a) The manipulation of the BFP with grating wave vectors in the x-direction and (b) the focal point position, showing (i) the focus on the center of grating material and (ii) the focus on the center of the sample

The BFP image in the case of a grating sample would be calculated as follows;

(1) Calculate the reflection coefficient from the RCWA. The reflection coefficient contains the mth set, so calling the reflection coefficient at any mth order with $r_{s,mth}$ and $r_{p,mth}$.

(2) Calculate the electric field components. It needs to point out that the reflection coefficient of p-polarization in the RCWA has been calculated from the magnetic field, so the reflection coefficient of p-polarization must be multiplied with $-i/n_0$ to change into an electric field.

$$E_{x,mth} = \frac{-i}{n_0} r_{p,,mth} \cos(\varphi) - r_{s,mth} \sin(\varphi) \tag{1.5}$$

$$E_{y.mth} = \frac{-i}{n_0} r_{p,mth} \sin(\varphi) + r_{s,mth} \cos(\varphi) \tag{1.6}$$

(3) Calculate the total wave vector in the x-direction ($k_{xtotal,m}$) at any mth diffraction order.

$$k_{xtotal,m} = k_x + k_{g,m} = k_x + m\frac{2\pi}{\lambda_g} \tag{1.7}$$

where, grating order m = -mth, …, -2, -1, 0, 1, 2, …, mth and λ_g is grating period.

(4) Calculate the total electric field component in the x-direction (E_{xtotal}) by summing every electric field diffraction order, accounting the focal point at x position (x_{pos}) and phase shift (β_{mth}).

$$\beta_{mth} = \exp(i(k_x - k_{xtotal,mth})x_{pos}) \tag{1.8}$$

$$E_{xtotal} = \sum_{-mth}^{mth} E_{x,mth}\beta_{mth} \tag{1.9}$$

(5) Calculate the total electric field component in the y-direction (E_{ytotal}) with the same method described in (4).

$$E_{ytotal} = \sum_{-mth}^{mth} E_{y,mth}\beta_{mth} \tag{1.10}$$

(6) Calculate the BFP with a grating sample by

$$BFP_{grating} = \left|E_{xtotal}\right|^2 + \left|E_{ytotal}\right|^2 \quad (1.11)$$

4. Results and Discussion

4.1 The Back Focal Plane image with grating sample

In this section, the result of implementing the BFP image of the grating-assisted SP sensor-based Kretschmann configuration is shown in Figure 5. The structure details of the sensor were 48 nm gold (n_{gold}=0.18344-3.4332*i* (Johnson & Christy, 1972), 800 nm Polymethyl methacrylate (PMMA) grating thickness (n_1=1.483 (Zhang et al., 2020) with 800 nm grating period and 240 nm grating width. Note that the focal point position focused on half of the grating period, and structure details were found in (Sasivimolkul et al., 2021).

Figure 5 shows the BFP image with the SPR mode and Fabry-Perot (FP) mode (Rao, 2006) in the p-polarization direction. In our previous work, the authors reported FP mode excitation in a grating thin-film-based SP sensor (Sasivimolkul et al., 2021). The FP resonant mode is formed by the sub-wavelength grating condition (Mateus et al., 2004). The grating layer made itself a resonant layer. The two reflected lights interfered with performing the FP resonant condition upon incident light impact onto the interface between gold/PMMA and PMMA/sample. The FP resonant mode's significant characteristic was a narrow response dip, which increased the sensor's quality.

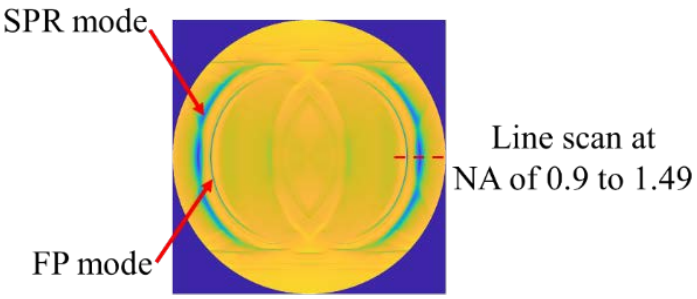

Figure 5 The calculated BFP image with a grating sample in the air with 1.49 NA objective lens, showing the SPR mode and FP mode in the p-polarization direction.

The different focal point position gives the different BFP respond. The different focal point positions at (i) the center of grating material and (ii) the center of a sample have been shown in Figure 4(b) will be studied. Line scan images for NA of 0.9 to 1.49 as depicted as a dashed red line in Figure 5 were computed for different grating periods as shown in Figure 6(a) for case (i) and Figure 6(b) for case (ii). The different focal point positions gave a different amplitude or reflectance, as seen when a grating period was more than around 1 μm. Both SPR and FP mode had a shallow reflectance in the center of the grating, in contrast to the center of the sample was still a deep reflectance.

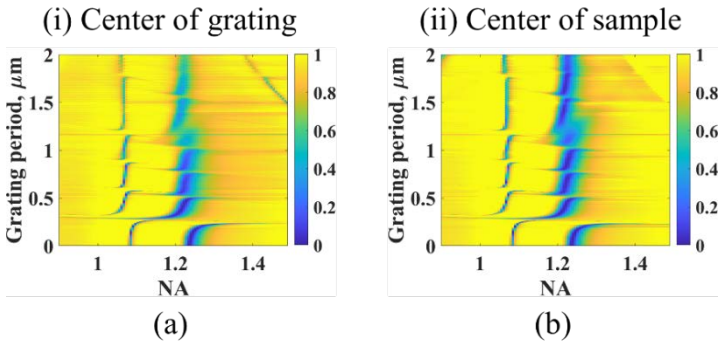

Figure 6 The line scan of Figure 5 in the function of varying grating periods at a different focal point; (a) the focus is on a center of a grating and (b) the focus is on a center of a sample.

4.2 Refractive index sensing application

In refractive index sensing, the SPR mode and FP mode in Figure 5 could be used as a sensor (Liao et al., 2012) because they possess refractive index sensitivity. If the air was replaced by nitrogen gas, water, and protein, the responses dip shifted to higher NA.

The authors then compared a line scan response from BFP images of the conventional SP sensor and the grating-assisted SP sensor (structure detail in section 4.1), with the refractive index of glucose at different concentrations as shown in Table 1 obtained in (Robinson & Dhanlaksmi, 2017). Figure 7 shows the line scan response with the change in the refractive index of sample 0.001 RIU (refractive index unit) to demonstrate a response dip between the sensor with grating and without grating. The grating-assisted SP sensor's response dips were separate from each other obviously, whereas the response dips of a sensor without grating were mostly overlaid together.

Table 1 Glucose concentration and its refractive index

Glucose concentration, g/dl	Refractive index
0 to 0.015	1.335±0.001
0.625	1.336±0.001
1.25	1.337±0.001
2.5	1.338±0.001
5	1.341±0.001

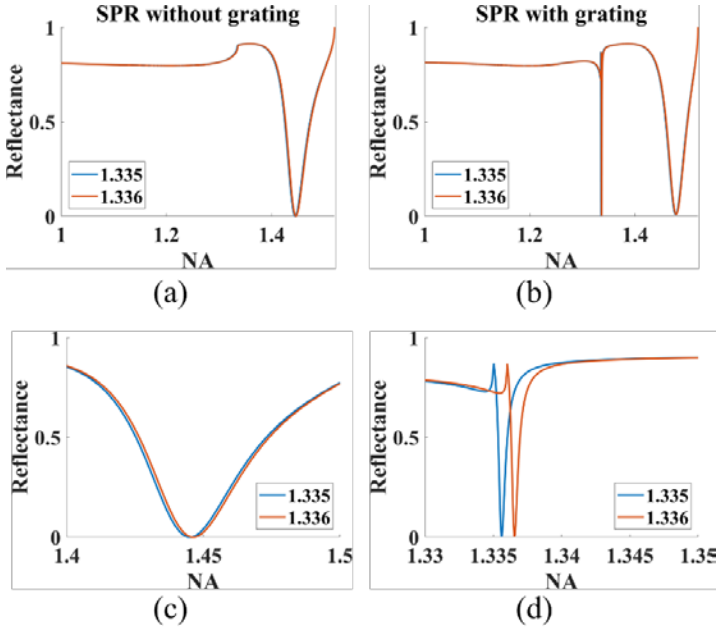

Figure 7 the line scan response in intensity ($|r_p|^2$) of the SP sensor (a) without and (b) with grating. (c) and (d) shows zoomed image of (a) and (b), respectively

Qualitative parameters measured from a response dip for comparison, including sensitivity, full-width at half maximum (FWHM), FoM, and dynamic range (DR), will be shown in Table 2.

- Sensitivity is defined as a change in respond dip position divided by a change in the refractive index of an analyte.
- FWHM is defined as a width of response signal at half amplitude (at 0.5 reflectances).
- FoM is defined as sensitivity divided by FWHM.
- DR is defined as a range of the value indicating the range of refractive indices, which the sensor can measure under defined condition; the reflectance of respond dip of a resonant mode must be less than 0.25. Note that the refractive index of sample variation from 1 to 1.45 to measure the DR.

Table 2 A comparison of SP sensor with and without grating

Structure	Sensitivity	FWHM	FoM	DR
SP sensor without grating	1.188	0.035	34	1.00 - 1.40
SP sensor with grating	0.724	0.0012	603	1.00 - 1.38

Table 2 shows that the SP sensor with grating on the surface has a narrow FWHM and high FoM but needs to trade-off a sensing area with a grating material, reducing the sensitivity. However, it gives a better quality around 20 times with an equally dynamic range.

5. Conclusion

Since the back focal plane analysis has been a potential tool to analyze material properties on the surface plasmon sensor or refractive index sensing. This paper shows the calculation method for simulating the back focal plane image with and without the grating sample and also presents the difference of BFP with different focal point positions. This calculation method can be a back focal plane image generator for machine learning in the optics field.

6. Acknowledgements

This work was funded by the Research Institute of Rangsit University. We would like to acknowledge the Biophysics and Medical Optic laboratory, College of Biomedical Engineering, to support facilities during research.

7. References

Couture, M., Zhao, S. S., & Masson, J.-F. (2013). Modern surface plasmon resonance for bioanalytics and biophysics. *Physical Chemistry Chemical Physics*, *15*(27), 11190-11216.

Dai, Y., Xu, H., Wang, H., Lu, Y., & Wang, P. (2018). Experimental demonstration of high sensitivity for silver rectangular grating-coupled surface plasmon resonance (SPR) sensing. *Optics Communications*, *416*, 66-70. https://doi.org/https://doi.org/10.1016/j.optcom.2018.02.010

Gittes, F., & Schmidt, C. F. (1998). Interference model for back-focal-plane displacement detection in optical tweezers. *Optics letters*, *23*(1), 7-9.

Homola, J., Koudela, I., & Yee, S. S. (1999). Surface plasmon resonance sensors based on diffraction gratings and prism couplers: sensitivity comparison. *Sensors and Actuators B: Chemical*, *54*(1-2), 16-24.

Hu, C. (2011). Surface plasmon resonance sensor based on diffraction grating with high sensitivity and high resolution. *Optik*, *122*(21), 1881-1884.

Johnson, P. B., & Christy, R. W. (1972). Optical Constants of the Noble Metals. *Physical Review B*, *6*(12), 4370-4379. https://doi.org/10.1103/PhysRevB.6.4370

Johnsson, B., Löfås, S., & Lindquist, G. (1991). Immobilization of proteins to a carboxymethyldextran-modified gold surface for biospecific interaction analysis in surface plasmon resonance sensors. *Analytical biochemistry*, *198*(2), 268-277.

Kretschmann, E., & Raether, H. (1968). Radiative decay of non-radiative surface plasmons excited by light. *Z. Naturforsch. a*, *23*(12), 2135-2136.

Liao, C., Hu, T., & Wang, D. (2012). Optical fiber Fabry-Perot interferometer cavity fabricated by femtosecond laser micromachining and fusion splicing for refractive index sensing. *Optics Express*, *20*(20), 22813-22818.

Mahmoudpour, M., Ezzati Nazhad Dolatabadi, J., Torbati, M., & Homayouni-Rad, A. (2019). Nanomaterials based surface plasmon resonance signal enhancement for detection of environmental pollutions. *Biosensors and Bioelectronics*, *127*, 72-84. https://doi.org/https://doi.org/10.1016/j.bios.2018.12.023

Mann, C. J., Yu, L., Lo, C.-M., & Kim, M. K. (2005). High-resolution quantitative phase-contrast microscopy by digital holography. *Optics Express*, *13*(22), 8693-8698.

Mateus, C. F., Huang, M. C., Deng, Y., Neureuther, A. R., & Chang-Hasnain, C. J. (2004). Ultrabroadband mirror using low-index cladded subwavelength grating. *IEEE Photonics Technology Letters*, *16*(2), 518-520.

Moharam, M., Grann, E. B., Pommet, D. A., & Gaylord, T. (1995). Formulation for stable and efficient implementation of the rigorous coupled-wave analysis of binary gratings. *JOSA a*, *12*(5), 1068-1076.

Nelson, B. P., Frutos, A. G., Brockman, J. M., & Corn, R. M. (1999). Near-infrared surface plasmon resonance measurements of ultrathin films. 1. Angle shift and SPR imaging experiments. *Analytical Chemistry*, *71*(18), 3928-3934.

Nugent-Glandorf, L., & Perkins, T. T. (2004). Measuring 0.1-nm motion in 1 ms in an optical microscope with differential back-focal-plane detection. *Optics letters*, *29*(22), 2611-2613.

Otto, A. (1968). A new method for exciting non-radioactive surface plasma oscillations. *phys. stat. sol*, *26*, K99-K101.

Pechprasarn, S., & Albutt, N. (2019). Multiple Reflections Modeling for Multi-Layered Optical Structures. Applied Mechanics and Materials,

Pechprasarn, S., Ittipornnuson, K., Jungpanich, T., Pensupa, N., & Albutt, N. (2019). Surface Plasmon Biosensor Platform for Food Industry. *Applied Mechanics and Materials*, *891*, 103-108. https://doi.org/10.4028/www.scientific.net/AMM.891.103

Pechprasarn, S., & Somekh, M. (2012). Surface plasmon microscopy: resolution, sensitivity and crosstalk. *Journal of Microscopy*, *246*(3), 287-297.
Pechprasarn, S., & Somekh, M. G. (2014). Detection limits of confocal surface plasmon microscopy. *Biomedical optics express*, *5*(6), 1744-1756.
Pechprasarn, S., Zhang, B., Albutt, D., Zhang, J., & Somekh, M. (2014). Ultrastable embedded surface plasmon confocal interferometry. *Light: Science & Applications*, *3*(7), e187-e187. https://doi.org/10.1038/lsa.2014.68
Rao, Y.-J. (2006). Recent progress in fiber-optic extrinsic Fabry–Perot interferometric sensors. *Optical Fiber Technology*, *12*(3), 227-237.
Ritchie, R. H., Arakawa, E., Cowan, J., & Hamm, R. (1968). Surface-plasmon resonance effect in grating diffraction. *Physical Review Letters*, *21*(22), 1530.
Robinson, S., & Dhanlaksmi, N. (2017). Photonic crystal based biosensor for the detection of glucose concentration in urine. *Photonic Sensors*, *7*(1), 11-19. https://doi.org/10.1007/s13320-016-0347-3
Rothenhäusler, B., & Knoll, W. (1988). Surface–plasmon microscopy. *Nature*, *332*(6165), 615-617.
Sasivimolkul, S., Pechprasarn, S., & Somekh, M. G. (2021). Analysis of open grating based Fabry-Pérot resonance structures with potential applications for ultrasensitive refractive index sensing. *IEEE Sensors Journal*, 1-1. https://doi.org/10.1109/JSEN.2021.3063136
Schasfoort, R. B. (2017). *Handbook of surface plasmon resonance*. Royal Society of Chemistry.
Shen, M., Chow, T. W. K., Shen, H., & Somekh, M. G. (2020). Virtual optics and sensing of the retrieved complex field in the back focal plane using a constrained defocus algorithm. *Optics Express*, *28*(22), 32777-32792. https://doi.org/10.1364/OE.404573
Stabler, G., Somekh, M. G., & See, C. (2004). High-resolution wide-field surface plasmon microscopy. *Journal of Microscopy*, *214*(3), 328-333.
Suvarnaphaet, P., & Pechprasarn, S. (2018). Enhancement of Long-Range Surface Plasmon Excitation, Dynamic Range and Figure of Merit Using a Dielectric Resonant Cavity. *Sensors*, *18*(9), 2757. https://www.mdpi.com/1424-8220/18/9/2757
Thillaivinayagalingam, P., Gommeaux, J., McLoughlin, M., Collins, D., & Newcombe, A. R. (2010). Biopharmaceutical production: Applications of surface plasmon resonance biosensors. *Journal of Chromatography B*, *878*(2), 149-153. https://doi.org/https://doi.org/10.1016/j.jchromb.2009.08.040
Zhang, X., Qiu, J., Li, X., Zhao, J., & Liu, L. (2020). Complex refractive indices measurements of polymers in visible and near-infrared bands. *Applied Optics*, *59*(8), 2337-2344. https://doi.org/10.1364/AO.383831